




## Triangular and Quadrilateral Bézier Discretizations of Trimmed CAD Surfaces and Its Application to the Isogeometric Analysis

Xiaoxiao Du<sup>1,a</sup> , Gang Zhao<sup>2,a,b</sup>, Wei Wang<sup>3,a</sup>, Mayi Guo<sup>4,a</sup>, Ran Zhang<sup>5,a</sup>, Jiaming Yang<sup>6,a</sup>

<sup>a</sup>School of Mechanical Engineering and Automation, Beihang University, Beijing, PR China,

<sup>b</sup>Beijing Engineering Technological Research Center of High-Efficient & Green CNC Machining Process, Beijing, PR China,

<sup>1</sup>Beihang University, [duxiaoxiao@buaa.edu.cn](mailto:duxiaoxiao@buaa.edu.cn)

<sup>2</sup>Beihang University, [zhaog@buaa.edu.cn](mailto:zhaog@buaa.edu.cn)

<sup>3</sup>Beihang University, [jrrt@buaa.edu.cn](mailto:jrrt@buaa.edu.cn)

<sup>4</sup>Beihang University, [windowsgmy@126.com](mailto:windowsgmy@126.com)

<sup>5</sup>Beihang University, [feliciamail@buaa.edu.cn](mailto:feliciamail@buaa.edu.cn)

<sup>6</sup>Beihang University, [williamyj@163.com](mailto:williamyj@163.com)

Corresponding author: Wei Wang, [jrrt@buaa.edu.cn](mailto:jrrt@buaa.edu.cn)

**Abstract.** Isogeometric analysis on complex geometries built with trimmed NURBS patches has always been regarded as a laborious challenge for practitioners. In this paper, trimmed NURBS surfaces are converted into mixed-Bézier meshes consisting of tensor-product (rectangular) Bézier patches and triangular Bézier patches for isogeometric analysis. It provides an advisable method to analyze topology-complex geometries with an isogeometric approach. The converted model is watertight and keeps the original surfaces unchanged except the narrow areas along the trimming curves. Several numerical examples including 2D elasticity, free vibration of plate and static bending of shell are investigated to verify the validity of the proposed method.

**Keywords:** trimmed NURBS surfaces, mixed Bézier elements, watertight model, isogeometric analysis

**DOI:** <https://doi.org/10.14733/cadaps.2021.738-759>

## 1 INTRODUCTION

In traditional engineering product development process, design is fulfilled in CAD systems and analysis is implemented in FEA frameworks. Since FEA emerged before CAD, mesh structures have been employed in FEA to represent geometries and drive analysis, even though afterwards NURBS has been widely used and gradually became the foundation of geometrical modeling in CAD systems. Therefore, CAD geometries

should be converted into analysis-suitable mesh models for finite element analysis and this conversion process consumes up to 80% of the overall analysis time and thus is considered to be a major impediment to the integration of CAD and FEA [5]. As a consequence, the efficiency of engineering product development process is dramatically reduced. Under these circumstances, isogeometric analysis (IGA) is proposed by Thomas J. R. Hughes aiming to realize the in-depth integration of CAD and FEA through employing the basis functions in CAD geometries to interpolate field variables in FEA [13].

NURBS unifies conic and free-form geometrical representation and is equipped with a series of elegant properties and powerful algorithms, thus holds a dominant position in CAGD field [22]. NURBS surfaces are based on a tensor-product structure and the intersection of two surfaces is very complex. Therefore, it also has drawbacks, e.g., interface gap and local refinement, which have always been tolerated due to the irreplaceable position of NURBS in geometrical representation. The capacity of representing complex geometries is restricted by the tensor-product topological structure of NURBS. Designers usually glue multiple surfaces and trim off unwanted parts to construct complicated geometries in CAD systems. As shown in Fig. 1, an automobile fender model consists of 462 NURBS surfaces where 253 surfaces are trimmed. Figure 1(a) shows the transparent rendering of the initial 462 NURBS surfaces without trimming. Figure 1(b) presents the rendering of the resulted trimmed surfaces and untrimmed surfaces in CATIA. Solid lines denote the boundaries of trimmed and untrimmed surfaces while dashed lines denote screened boundaries. Blown-up views present the detailed trimming information in red boxes. However, trimming and gluing in CAD models may introduce drawbacks like gap, overlapping and non-conforming, between different patches. Here the defect of non-conforming means that the adjacent boundary curves with the same geometrical shape have different degrees or knot vectors. These drawbacks will place obstacles in the way of downstream applications including computational analysis, numerical control machining, geometrical rendering, 3D printing. For example, non-conforming problems will affect the stiffness matrix assembling and patches coupling, which means extra works are required to solve these problems [6, 7, 39]. In this paper, we focus on isogeometric analysis of complicated CAD geometries built with trimmed multi-patch NURBS surfaces, as a general way to optimize the trimmed model for IGA's exertion, or as the first step for using IGA in occasions demanding more faithful shape fidelity, like in sheet metal forming simulation's contact calculation.

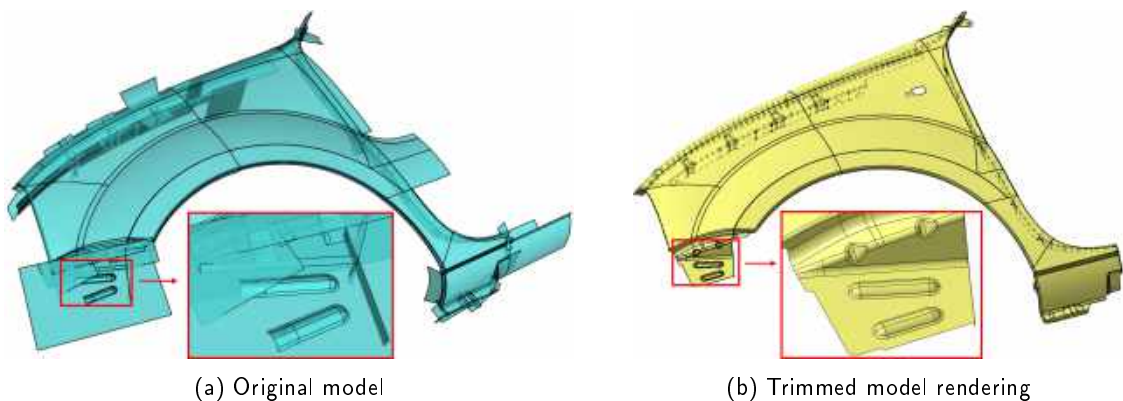


**Figure 1:** Automobile fender model is built with 462 NURBS surfaces where 253 surfaces are trimmed.

Isogeometric analysis of trimmed geometries is a valuable topic and full of challenges, due to the fact that trimming features are widely used but extremely sophisticated. The first work on isogeometric analysis of 2D trimmed NURBS surface is presented by Kim et al. [15, 16], who employed NURBS-enhanced integration scheme [28] for integration of trimmed NURBS elements. A similar problem is also investigated in [33] for compound B-spline surfaces based isogeometric analysis. Schmidt et al. [26] reconstructed the trimmed

element with a tensor-product Bézier patch and established the transformation matrix between the control points of untrimmed surface and the reconstructed Bézier patch through the selected sampling points. The so-called nested Jacobian approaches (NEJA) are proposed by Breitenberger et al. [2] from the same team to parameterize the trimmed domain which is decomposed into several subsets for isogeometric analysis of shell structures [21]. Beer et al. [1] presented a double mapping method for analysis of trimmed CAD surfaces by establishing the mapping from the trimming domain to a rectangular parametric element. Ruess et al. employed finite cell method (FCM) to deal with the trimming problem [24, 25]. Nagy and Benson [20] approximated the trimmed element with refined control polygons of its boundary curves and established a quadrature rule on the approximated polygon. Marussig et al. gave an excellent review of isogeometric analysis of trimmed CAD models and divided the current approaches into global and local [18]. A concept of extended B-splines is developed to provide a stable basis for isogeometric analysis of trimmed geometries [19]. Zhu et al. developed a so-called B++ splines to represent the trimmed NURBS for isogeometric analysis [40]. Xia and Qian [34, 35] converted trimmed CAD surfaces into watertight geometry represented by rational triangular Bézier splines (rTBS) for the subsequent volumetric discretization process. Xu et al. improved the method proposed by Kim [16] to solve trimmed problems more efficiently [38]. Buffa et al. proposed a stabilized approach for isogeometric analysis of trimmed geometries [3]. Thomas et al. developed a so-called, U-splines, to construct spline basis on the unstructured mesh and expected to bypass the limitation of traditional trimmed geometries in the analysis [29].

Considering the whole process of product development, the geometrical defects will affect the downstream applications (e.g., CAM, 3D printing) that need the use of geometries. Therefore, converting a trimmed CAD geometry into a watertight geometry without drawbacks of non-conforming, gap and overlap seems to be a superior approach for isogeometric analysis and other applications. In this paper, a novel method is proposed to solve the trimming problems by converting the trimmed NURBS surface geometry into watertight geometry, which is comprised of tensor-product Bézier patches and triangular Bézier patches. Most area of the trimmed surface is exactly preserved and only the narrow area along the trimming curves is approximated. It is easy to deal with multiple trimmed NURBS surface models without additional processing on nonconforming problems. Moreover, compared with the method proposed by Xia [34], trimming curves can be explicitly expressed so that boundary conditions could be expediently enforced. The order of the converted watertight model could keep consistent with the order of the original trimmed model.

The paper is organized as follows. Section 2 begins by reviewing Bernstein-Bézier foundations. Section 3 presents the definition and generation of trimming surface. The detailed process of converting trimmed NURBS surfaces into mixed Bézier patches is described in Section 4. Elasticity governing equations and isogeometric discretizations are briefly introduced in Section 5. Several numerical examples including 2D elasticity problems, plate and shell problems are investigated in Section 6 to verify the proposed method. In section 7, a short conclusion and outlook for future works are presented.

## 2 PRELIMINARIES ON BERNSTERIN-BÉZIER REPRESENTATION

Bernstein polynomial basis was firstly proposed by Sergei Natanovich Bernstein in 1912 to approximate the continuous functions by polynomials, even though it has been proved to be versatile in interactive design of polynomial functions after several decades [12]. The univariate Bernstein basis functions of degree  $n$  on  $t \in [0, 1]$  are given as

$$B_i^n(t) = \binom{n}{i} t^i (1-t)^{n-i}, \quad i = 0, 1, \dots, n. \quad (1)$$

By defining  $u = t, v = 1 - t$ , it can also be rewritten as

$$B_{ij}^n(u, v) = \frac{n!}{i!j!} u^i v^j, \quad 0 \leq i, j \leq n, i + j = n, \quad (2)$$

where  $u, v$  are called *barycentric coordinates*. The multivariate extension is obvious and natural with the definition of univariate Bernstein basis in Eqs. (1) and (2). The barycentric coordinates version of Bernstein basis can also be extended and used in triangular Bézier patch. A polynomial of Bernstein form associated with arbitrary coefficients  $c_i, i = 0, 1, 2, \dots, n$  is defined by

$$f^n(t) = \sum_{i=0}^n c_i B_i^n(t), \quad t \in [0, 1]. \quad (3)$$

The Bernstein-form polynomials inherit some attractive properties from Bernstein basis functions such as symmetry, non-negativity, partition of unity, recursion and numerical stability. Meanwhile, some concise and efficient algorithms of Bernstein basis like degree elevation, derivatives, integrals and arithmetic operations will bring conspicuous convenience of calculation to polynomials in Bernstein form, thus they have been widely applied in CAGD, computer graphics and finite element analysis.

The univariate Bernstein basis function in Eq. (2) can be extended to bivariate function defined over the triangle  $\mathcal{T}$  as

$$B_{ijk}^n(u, v, w) = \frac{n!}{i!j!k!} u^i v^j w^k, \quad 0 \leq u, v, w \leq 1, u + v + w = 1 \quad (4)$$

with  $0 \leq i, j, k \leq n, i + j + k = n$ . Given a set of vector-valued control points  $\mathbf{b}_{ijk}$ , a triangular Bézier surface  $\mathbf{T}$  in physical domain mapping from the parametric domain  $\mathcal{T}$ , can be written as

$$\mathbf{T}(u, v, w) = \sum_{i+j+k=n} \mathbf{b}_{ijk} B_{ijk}^n(u, v, w). \quad (5)$$

Besides triangular Bézier surface, tensor-product Bézier surface is another popular surface based on Bernstein basis function and can be defined as

$$\mathbf{S}(u, v) = \sum_{i=0}^n \sum_{j=0}^m B_i^n(u) B_j^m(v) \mathbf{b}_{i,j}, \quad 0 \leq u, v \leq 1, \quad (6)$$

where  $B_i^n(u)$  and  $B_j^m(v)$  are the univariate Bernstein basis functions in two directions,  $m, n$  denote the degrees,  $\mathbf{b}_{i,j}$  are the surface control points. As an example, figure 2 shows basis functions and control nets of a cubic triangular Bézier surface and a bi-cubic tensor-product Bézier surface. For more details about Bernstein basis, triangular and tensor-product Bézier surfaces, we refer readers to [22].

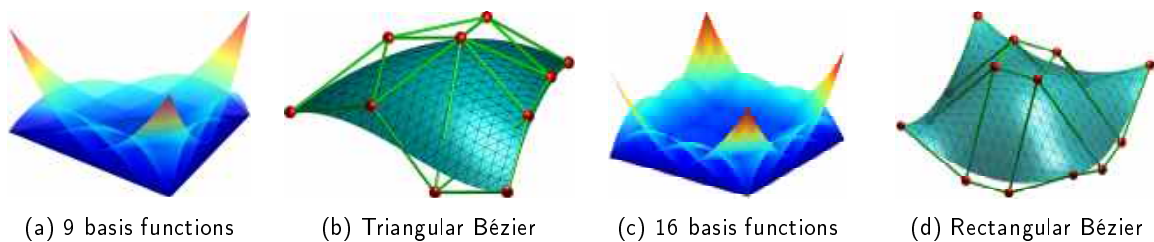


**Figure 2:** Basis functions and control nets of a cubic triangular Bézier surface and bi-cubic tensor-product Bézier surface.

### 3 TRIMMING PROBLEMS

#### 3.1 Trimming Surface Definition

The rectangular topology structure of NURBS has limited its capacity on representing complicated geometries. To simplify the representation of NURBS-based complex geometries, trimming surface is defined on NURBS parametric space by specifying a valid domain  $\Omega_v$ , which is constituted by a closed outer boundary curve and several closed inner boundary curves. Assuming that the domain enclosed by outer boundary curve is denoted by  $\Omega_{out}$  and the  $i$ -th domain enclosed by inner boundary curve is denoted by  $\Omega_{in}^i$ , then

$$\Omega_v = \Omega_{out} - \sum_i \Omega_{in}^i.$$

In the definition of trimming surface, the left side of trimming boundaries is assumed as valid. Therefore, the outer trimming boundary is defined as counter-clockwise and inner trimming boundaries are clockwise. An example of trimming surface is given in Fig. 3. Red curve  $\mathbf{C}_{in}^p(\bar{t})$  and blue curve  $\mathbf{C}_{out}^p(\bar{t})$  in Fig. 3(b) denote the inner trimming boundary curve and outer trimming boundary curve in parametric space, respectively.  $\mathbf{C}_{in}^s(t)$  and  $\mathbf{C}_{out}^s(t)$  in Figs. 3(c) denote the related mapping curves in physical space. Substituting the parametric curve  $\mathbf{C}^p(\bar{t})$  into the surface  $\mathbf{S}(u, v)$ , the mapping curve  $\mathbf{C}^s(\bar{t})$  can be expressed as  $\mathbf{C}^s(\bar{t}) = \mathbf{S}(\mathbf{C}^p(\bar{t}))$ . Assuming that the degrees of the surface  $\mathbf{S}(u, v)$  are  $(d_u, d_v)$  and the degree of the parametric curve  $\mathbf{C}^p(\bar{t})$  is  $d_{\bar{t}}$ , then the degree of the resulted curve  $\mathbf{C}^s(\bar{t})$  is up to  $(d_u + d_v)d_{\bar{t}}$  [23]. So an approximated low-degree curve  $\mathbf{C}^s(t)$  is usually preferred to replace the exact high-order curve  $\mathbf{C}^s(\bar{t})$ . Unless otherwise instructed,  $t$  and  $\bar{t}$  hereafter denote the parameter of trimming curve in physical domain and parametric domain.  $u$  and  $v$  denote the two parameters of NURBS surface. Superscripts  $s$  and  $p$  denote the trimming curves in physical domain and parametric domain, respectively.

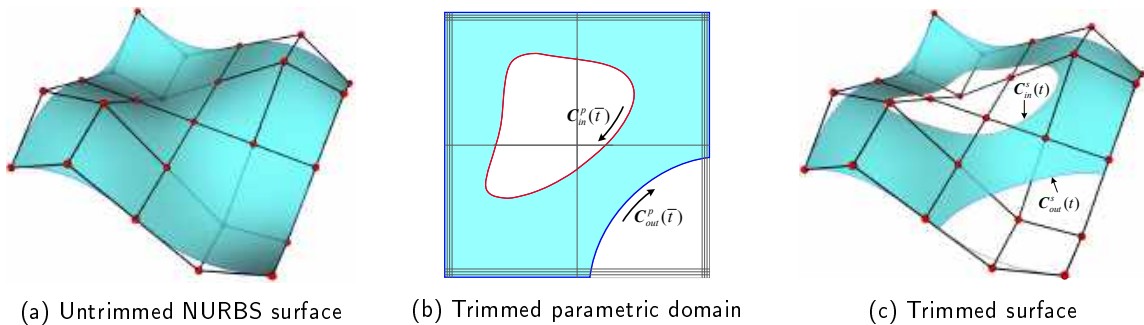


**Figure 3:** Trimmed NURBS surface. (a) initial untrimmed NURBS surface, (b) trimmed parametric domain and (c) the resulted trimmed surface mapping from the valid parametric domain.

#### 3.2 Surface to Surface Intersections

Trimming is closely linked to the surface to surface intersection (SSI) problem as illustrated in the Fig. 4(a). NURBS surface  $\mathbf{S}_1(u, v)$  is rendered in cyan and  $\mathbf{S}_2(u, v)$  is rendered in yellow.  $\mathbf{S}_1(u, v)$  and  $\mathbf{S}_2(u, v)$  intersect and result in a NURBS curve  $\mathbf{C}^s(t)$ . The resulted object in Fig. 4(b) is obtained by deleting the upper part of  $\mathbf{S}_2(u, v)$  and the off-paper part of  $\mathbf{S}_1(u, v)$ . In practice, exact calculation of the intersection curve  $\mathbf{C}^s(t)$  is computationally expensive and numerically unstable because the order of the resulted curve might be extremely high and could not be easily processed in CAX systems. For example, two bi-cubic surfaces will result in a curve of degree 324 [27]. Therefore, the intersection curve is usually approximated by a reasonable low-order

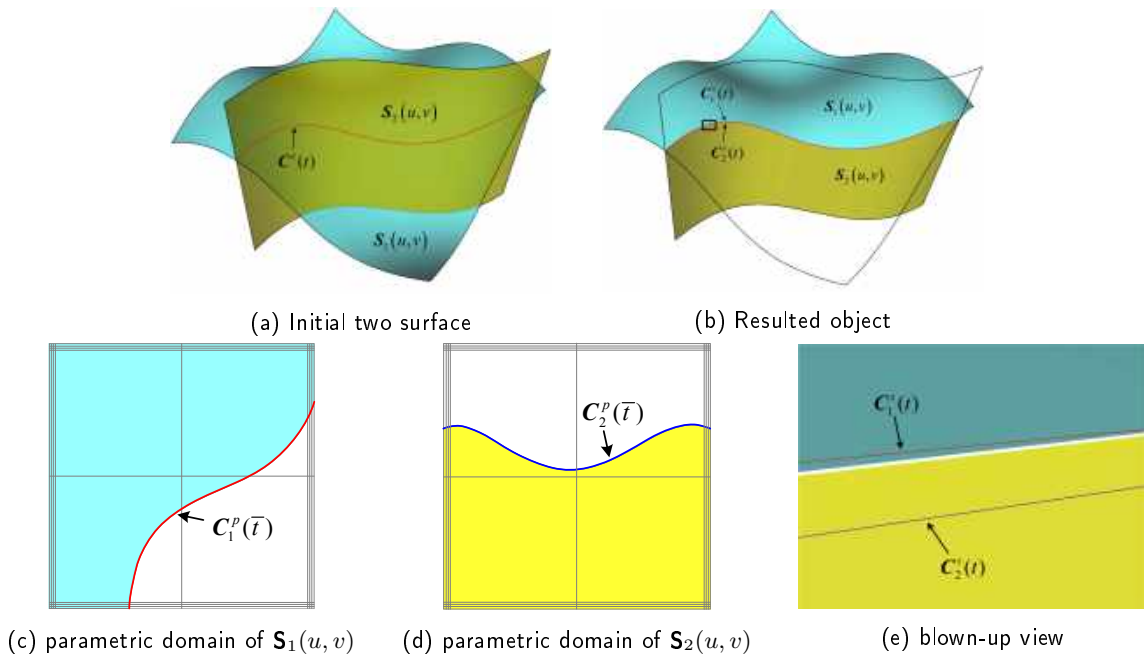


**Figure 4:** Surface to surface intersection. (a) initial two untrimmed surfaces and their intersection curves, (b) resulted object after trimming, (c) and (d) two independent parametric domains of  $S_1(u, v)$  and  $S_2(u, v)$ , (e) blown-up view of the selected domain marked with black box in (b).

curve. To define the trimmed surfaces  $S_1(u, v)$  and  $S_2(u, v)$ ,  $C^s(t)$  is reversed into the parametric domain of  $S_1(u, v)$  and  $S_2(u, v)$ . Then the trimming parametric curves  $C_1^p(\bar{t})$  and  $C_2^p(\bar{t})$  are approximately calculated as shown in Figs. 4(c) and 4(d). Since the intersection curve  $C^s(t)$  and parametric curves  $C_1^p(\bar{t})$  and  $C_2^p(\bar{t})$  are approximate, overlap and gap, as presented in Fig. 4(e), will be introduced along the interface of surfaces  $S_1(u, v)$  and  $S_2(u, v)$ . It may not be difficult to comprehend why SSI problem is a basic problem in CAGD.

## 4 MIXED BÉZIER DISCRETIZATION

### 4.1 NURBS Elements Classification

According to the positional relationship between NURBS elements and trimming curves, NURBS elements on trimmed surface can be classified into valid elements, invalid elements and trimmed elements. Valid and invalid element are completely located within the valid domain or invalid domain of trimmed surface without intersecting with any trimming curves. Trimmed element indicates the element intersecting with trimming curves. As shown in Fig. 5(a), A, B and C denote valid element, invalid element and trimmed element, respectively. Here element includes parametric element and physical element, where parametric element denotes the grid generated by the knot lines and physical element is the resulted surface element mapping from parametric element.

As for trimmed elements, four common cases are considered as indicated in the left column of Fig. 5(b). These four cases can be extended to 16 templates as given in right four columns of Fig. 5(b). Each template corresponds to two different trimmed elements because trimming curve has two opposite directions and only the left-side domain of trimming curve is valid. Note that besides these four common cases, some rare cases will be found in some CAD models. For example, the trimming curve will be tangent to the boundaries of the

trimmed element. These cases should be treated specially and will not be detailedly described in this paper.

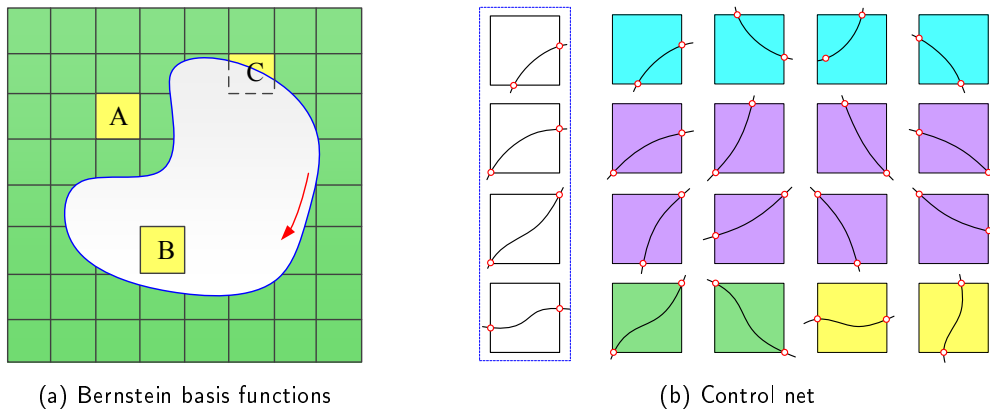


**Figure 5:** NURBS elements classification and templates of trimmed elements. (a) NURBS elements are classified into three categories: A-valid element, B-invalid element and C-trimmed element. (b) Trimmed elements further extend to 16 possible templates.

## 4.2 Trimmed Elements Detection

The category of the elements can be decided by the type of corresponding parametric element. Intersections between parametric trimming curves and parametric elements are computed to classify the elements. The detection of trimmed elements contains two tasks: first, the actual detection based on the knot lines and trimming curve  $\mathbf{C}^p$  intersections in the parameter space and second, the detection of the related curve segment of  $\mathbf{C}^s$  together with the projection of its knots  $t^s$  to the parameter space. Considering the example depicted in Fig. 4 the process of trimmed elements detection is described in detail as follows.

**Step 1:** Compute the intersection points  $\mathbf{P}(u_1^p, v_1^p)$  between knot lines and parametric trimming curve  $\mathbf{C}^p(\bar{t})$  in parametric domain. As illustrated in Figs. 6(a) and 6(c), red hollow dots denote the intersection points.

**Step 2:** Project the segment end points of  $\mathbf{C}^s(t)$  to parameter space. As presented in Figs. 6(b) and 6(d), blue square points denote the projected parameter points  $(u_2^p, v_2^p)$  in parametric domain. Assume that parameter points  $(u^p, v^p)$  consist of  $(u_1^p, v_1^p)$  and  $(u_2^p, v_2^p)$ .

**Step 3:** Determine the relationships between parameter points  $(u^p, v^p)$  and elements' parametric domain. If two or more than two parameter points  $(u^p, v^p)$  are on the border of an element or within an element, the element can be considered as a trimmed element.

All trimmed elements can be detected with the above three steps. It should be noticed that for the convenience of converting trimmed elements into mixed-Bézier patches, we also build the relationship between curve segments of physical trimming curve  $\mathbf{C}^s(t)$  and trimmed element. The trimming curve parameters  $t^s$  obtained from the projection of surface points  $\mathbf{S}(u_1^p, v_1^p)$  to  $\mathbf{C}^s(t)$  are inserted into  $\mathbf{C}^s(t)$ 's definition domain. The parameter points  $(u^p, v^p)$  are sorted according to the direction of  $\mathbf{C}^s(t)$ .

Valid elements and invalid elements can be distinguished by counting the number of intersections between a ray and trimming boundaries including outer trimming boundary curves and inner trimming boundary curves. In this paper, center point of the element and x-axis forward direction are selected as the start point and the direction of the ray. If the number of intersections is odd and the element is not a trimmed element, then the element can be considered as a valid element. Otherwise it is an invalid element. So far all elements might be classified.

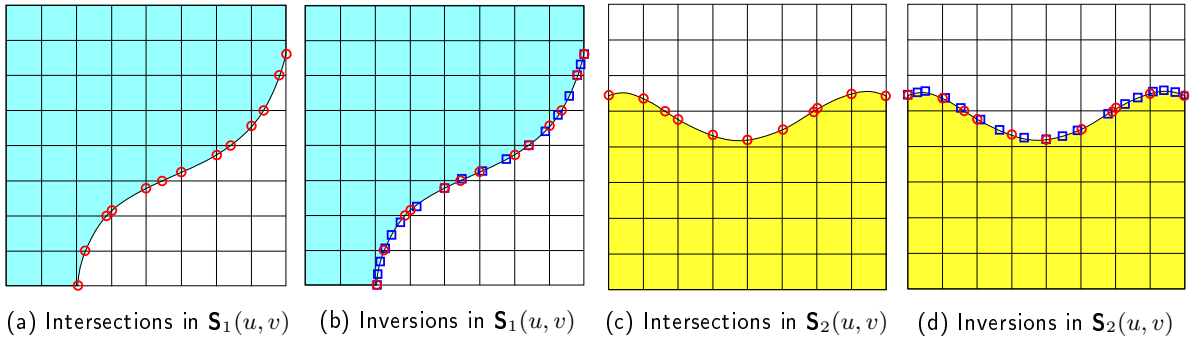


**Figure 6:** Trimmed elements detection in parametric domain. Red dots denote the intersections between knot lines and parametric trimming curves. Blue square points indicate the inversion points of segment points of physical trimming curve  $C^s$  in parametric domain.

### 4.3 Interface Conforming

Multiple trimmed NURBS surfaces are frequent in engineering model and the interfaces between adjacent surfaces are always inconsistent. Therefore, conforming problem has become a challenging and interesting problem in context of isogeometric analysis, and is widely investigated by using different methods to glue multiple untrimmed patches and trimmed patches [4, 6, 24, 39]. In this paper, the relationships between adjacent trimmed or untrimmed surfaces are analyzed firstly and then adjacent boundaries are conformed to build a watertight model. The algorithm of conforming operation can be depicted as follows.

**Step 1:** Iterate each boundary curve of trimmed surfaces and untrimmed surfaces to find the adjacent boundary curves. As illustrated in Fig. 7(a),  $C_1^s(t)$  and  $C_2^s(t)$  are two adjacent boundary curves.

**Step 2:** Compute all points corresponding to the parametric knot values of each curve and project them to current curve's adjacent curve. Record the parameters of the projected points and perform the knot insertion algorithm at the projected points.

**Step 3:** Replace the curve  $C_1^s(t)$  by  $C_2^s(t)$  to make sure the adjacent boundaries of adjacent surfaces are unanimous.

The conforming operation is naturally the knot insertion of adjacent curves and can make sure that the resulted model is watertight and favorable for the IGA application.

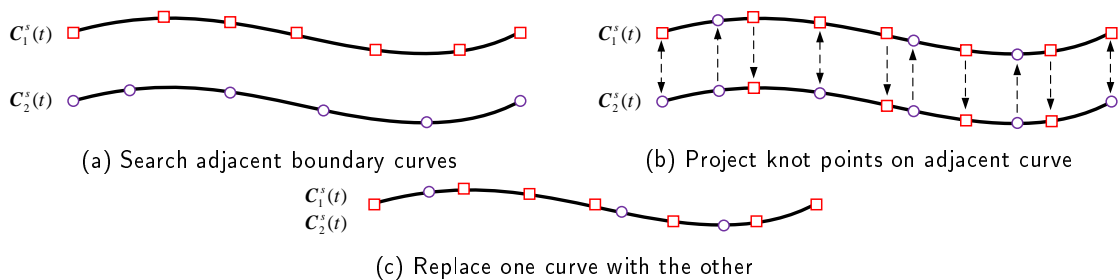


**Figure 7:** Boundary conforming operation.  $C_1^s(t)$  and  $C_2^s(t)$  are two adjacent boundary curves. Circular dots and square dots denote the physical points on boundary curves corresponding to the parametric knot values.



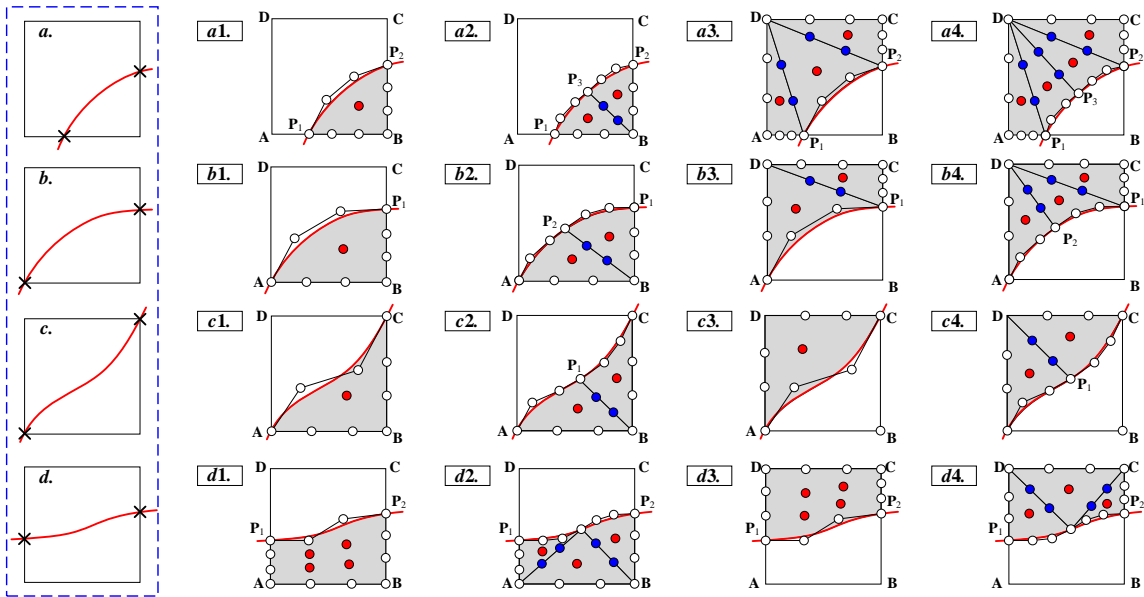


**Figure 8:** Conversion of a planar trimmed element into mixed Bézier patch. White dots denote the boundary control points which can be exactly extracted from existing boundaries of rectangular Bézier patch and physical trimming curves. Blue dots and red dots denote the approximated boundary control points and inner control points of converted Bézier patch, respectively. The degrees of surface and trimming curves are assumed to be 3.

#### 4.4 Bézier Elements Conversion from Trimmed Elements

In the process of converting trimmed NURBS surface to mixed Bézier patches, NURBS surface is firstly extracted as tensor product Bézier piecewise patches by using knot insertion algorithm. Bézier patches corresponding to valid elements are preserved and the patches related to invalid elements are removed. Now the problem is simplified as how to convert trimmed elements to mixed Bézier patches, which can be divided into two parts: boundary curves construction and inner control points generation.

##### 4.4.1 Construction of boundary curves

With algorithm of detecting the trimmed elements in previous subsection, it is easy to determine the relationship between Bézier segment curves on trimming curve and parametric points  $(u^p, v^p)$ , which can be sorted by the direction of the original trimming curves. The construction of boundary curves is performed in the physical space and a planar example is illustrated in Fig. 8 where four types of trimmed elements are considered. The valid domain in trimmed element can be directly substituted by one Bézier patch or further divided into sub-patches based on the distribution of trimming Bézier curve and parametric points  $(u^p, v^p)$  relevant with this element. For convenience of expression, red, blue and white circular dots denote the control points of the converted sub-patches in physical space, where white dots denote the boundary control points which can be exactly extracted from the existing boundaries of rectangular Bézier patch and physical trimming curves, blue dots and red dots denote the approximated boundary control points and inner control points of converted Bézier patch, respectively. The boundary curves of the sub-patches are firstly constructed and inner control points are subsequently generated.

Here **a1** and **a2** in type **a** are used as examples to portray the construction process of boundary curves. In case of **a1**, there is only one Bézier curve  $\widetilde{P_2P_1}$  included in the element. Bézier curve and element boundaries intersect at points  $P_2$  and  $P_1$ . Inserting parameters  $u^p$  or  $v^p$  of  $P_1$  and  $P_2$  into Bézier boundary curves  $\widetilde{AB}$  and  $\widetilde{BC}$ , we can obtain Bézier curves  $\widetilde{P_1B}$  and  $\widetilde{BP_2}$ . Then the three boundary curves  $\widetilde{P_2P_1}$ ,  $\widetilde{P_1B}$  and  $\widetilde{BP_2}$  will be employed as three edges of a triangular Bézier patch. It should be noticed that if the surfaces or trimming curves are rational, the weights of the control points corresponding to the intersected point  $P_1$  (or  $P_2$ ) in Bézier curves  $\widetilde{P_1B}$  (or  $\widetilde{BP_2}$ ) and  $\widetilde{P_2P_1}$  may be different and cannot be replaced by each other, because they are different in homogeneous coordinates even though they are the same in Euclidean coordinates. Therefore, we reparametrize the Bézier curve by changing the weights to obtain standard form of the Bézier curve. The reparametrization can be realized as follows [11],

$$\bar{\omega}_i = \left(\frac{\omega_0}{\omega_n}\right)^{\frac{i}{n}} \frac{\omega_i}{\omega_0}, \quad i = 0, 1, \dots, n, \tag{7}$$

where  $\omega_i$  and  $\bar{\omega}_i$  denote the weights of  $i$ -th control points for original Bézier curve and standard form, respectively. Then the weights of end control points  $\bar{\omega}_0 = \bar{\omega}_n = 1$ . After reparametrization, it is assured that the end control points of each boundary curve can be replaced by the adjacent one according to a prescribed error.

In case of **a2**, there are two Bézier curves  $\widetilde{P_1P_3}$  and  $\widetilde{P_3P_2}$  included in the element. The valid domain is considered to be divided into two triangular sub-patches. We firstly select some collocated parametric points on the parametric line  $\widetilde{BP_3}$  and compute the corresponding surface points, which are used to approximate a Bézier curve  $\widetilde{BP_3}$ . Now two triangular Bézier patches will be constituted from the boundary curves  $\widetilde{P_1B}$ ,  $\widetilde{BP_3}$ ,  $\widetilde{P_1P_3}$  and  $\widetilde{P_2B}$ ,  $\widetilde{BP_3}$ ,  $\widetilde{P_3P_2}$ . Similarly, a quadrilateral Bézier patch will be generated from four Bézier boundary curves  $\widetilde{AB}$ ,  $\widetilde{BP_2}$ ,  $\widetilde{P_2P_1}$  and  $\widetilde{P_1A}$  in case of **d1**. In the following, we will discuss how to construct triangular Bézier patch and quadrilateral Bézier patch from the obtained boundary curves.

#### 4.4.2 Inner control points generation

The construction of inner control points is based on the discrete Coons method proposed in [10], which is also employed and extended to construct B-spline volume [36, 37], because of its simplicity and validity.

For triangular Bézier patch, the inner control points can be built by using a mask of the form [10]

$$\begin{array}{ccccccc}
 & & & & \alpha & & \\
 & & & & \beta & & \beta \\
 & & & & \beta & & \beta \\
 & & & & \bullet & & \\
 & & & & \beta & & \beta \\
 & & & & \alpha & & \alpha
 \end{array} \tag{8}$$

with  $3\alpha + 6\beta = 1$  and  $\alpha = -\frac{1}{6}$  is recommended in [10] and is also used in this paper. Then for cubic triangular Bézier patch, the inner control point  $\mathbf{b}_{111}$  can be expressed as:

$$\mathbf{b}_{111} = \frac{1}{4}(\mathbf{b}_{201} + \mathbf{b}_{102} + \mathbf{b}_{021} + \mathbf{b}_{012} + \mathbf{b}_{210} + \mathbf{b}_{120}) - \frac{1}{6}(\mathbf{b}_{300} + \mathbf{b}_{030} + \mathbf{b}_{003}), \tag{9}$$

which is also employed to construct the Bézier surface from the mesh model, e.g., so-called curved PN triangles [32]. For degree higher than cubic, the inner control points can be calculated by solving a linear equation which is formulated by applying the mask given in Eq. (8) to each inner control point.

For quadrilateral Bézier patch, the inner control points can be generated by [10]:

$$\mathbf{b}_{ij} = (1 - \frac{i}{n})\mathbf{b}_{0j} + \frac{i}{n}\mathbf{b}_{nj} + (1 - \frac{j}{m})\mathbf{b}_{i0} + \frac{j}{m}\mathbf{b}_{im} - \begin{bmatrix} 1 - i/n & i/n \end{bmatrix} \begin{bmatrix} \mathbf{b}_{00} & \mathbf{b}_{0m} \\ \mathbf{b}_{n0} & \mathbf{b}_{nm} \end{bmatrix} \begin{bmatrix} 1 - j/m & j/m \end{bmatrix}, \quad (10)$$

where  $\mathbf{b}_{0j}, \mathbf{b}_{nj}, \mathbf{b}_{i0}, \mathbf{b}_{im}, i = 0, 1, \dots, n, j = 0, 1, \dots, m$  denote control points of four boundary curves.  $\mathbf{b}_{ij}, 0 < i < n, 0 < j < m$  denote the inner control points.

As shown in Fig. 9 The trimmed NURBS surface model given in Fig. 4 can be converted into congregation of rectangular Bézier patches and triangular Bézier patches (simplified as mixed-Bézier patches) by using the above conversion methods. Figures 9(a) and 9(b) present converted mixed-Bézier model after conforming operation as described in previous subsection, i.e., the insertion of the Bézier patches' vertexes into the boundary curves and using the curves' Bézier knots as vertexes of new Bézier patches, then the interface conforming of these curves.

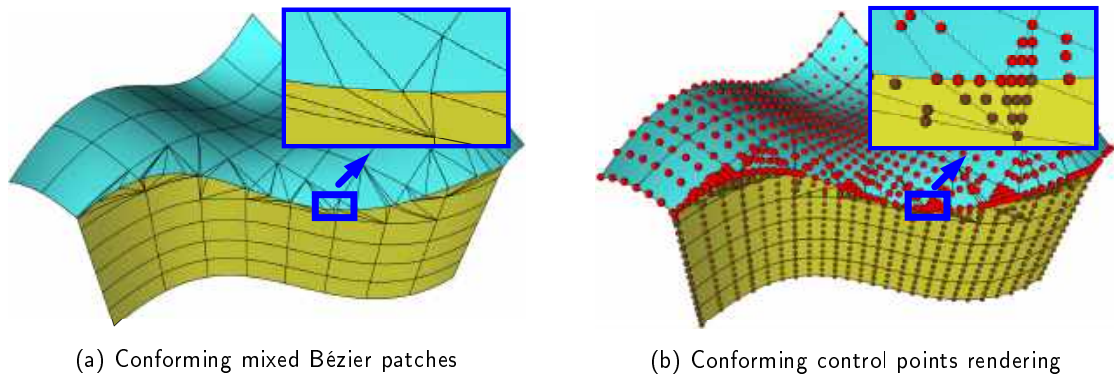


**Figure 9:** Conversion of trimmed NURBS models into mixed Bézier model. (a) The converted Bézier elements and (b) corresponding control points.

The approximation error occurs here, but it can be decreased with the refinement of the NURBS surface and in this paper it will not be discussed in full detail to avoid deviation from the main point. We notice that a Bézier projection method has been proposed to project any function including B-splines, NURBS, T-splines onto a local basis [30] and has been successfully utilized to project the NURBS or T-spline surface onto a collection of piecewise Bézier elements for further construction of geometrically exact volumetric Bézier mesh [9]. It will be interesting and helpful in the future to introduce the Bézier projection method into the mixed Bézier reconstruction from a trimmed Bézier patch.

#### 4.5 Boundary Optimization

In practical engineering model, the trimming boundary curves may include a variety of inner knots which will result in a lot of unwanted elements including some narrow elements. For example, as shown in Fig. 10(a), a regular surface rendered in Rhino is trimmed from the center by a projected circle and 60 triangular Bézier elements are generated as given in Fig. 10(b). It can be found that trimming curve includes an inner knots in each trimmed elements except four smaller trimmed elements. To reduce triangular Bézier elements generated by inner knots of a trimming curve, the trimming curve segments in any trimmed element are reparameterized into a very few consecutive Bézier curves. If the trimming curve segments located in a trimmed element are tangentially continuous, one Bézier curve is used for fitting. Otherwise the point where tangent vectors are discontinuous is used to divide curve segment into two parts for separately fitting. It should be noted that

one Bézier curve is usually enough to fit the curve segments in trimmed element since the element is relatively small after refining the NURBS surface for IGA. The classical least-square fitting method is employed in this paper. Figure 10(c) shows the converted mixed-Bézier model after boundary optimization. It can be found that the triangular Bézier elements are significantly reduced, which can alleviate the occurrence of ill-conditioned stiffness matrix in analysis. Improving the quality of generated triangular Bézier elements and meanwhile reducing the error of shape approximation is still an open question and needs further investigation.

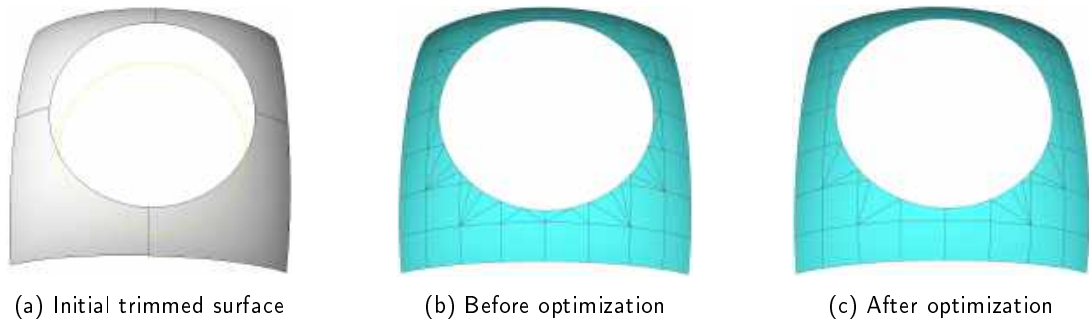


**Figure 10:** Initial trimmed NURBS surface and the converted mixed Bézier model before and after boundary optimization.

#### 4.6 Tank hanger example

A relatively complex model is presented here to verify the whole conversion process. As given in Fig. 11, a sheet metal part, tank hanger, is built with 125 NURBS surfaces where 65 surfaces are trimmed. Figure 11(a) presents the original model rendered in software Rhino and figure 11(b) shows the conforming mixed Bézier model obtained using our method. It can be found that there are several tiny and complex shaped surfaces at the corners of the tank hanger. To generate the conforming mixed Bézier model for isogeometric analysis, some surfaces are refined first to obtain suitable-size elements before the conversion. The mixed Bézier model presented in Fig. 11(b) consists of 2029 rectangular Bézier patches and 5082 triangular Bézier patches.

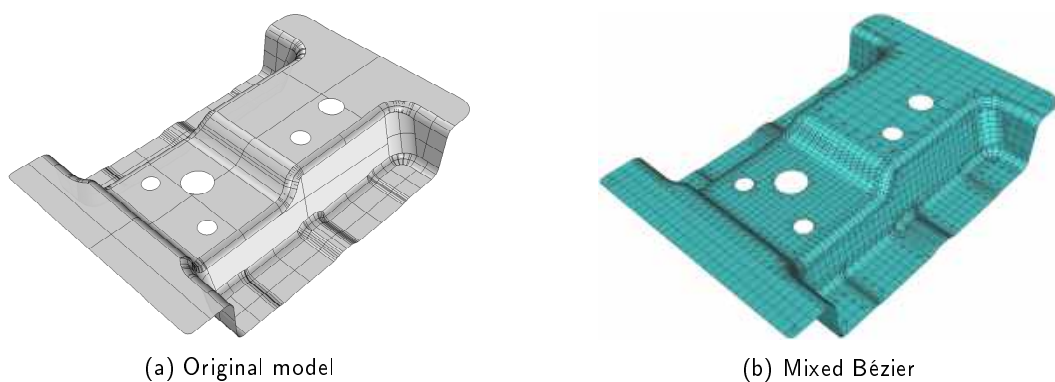


**Figure 11:** Tank hanger. (a) The original model rendered in Rhino and (b) mixed Bézier model obtained using our method.

## 5 ISOGOMETRIC FORMULATIONS

In this section, we will briefly discuss the isogeometric formulations for 2D elasticity problems and Reissner-Mindlin plate and shell elasticity problems, which will be addressed in the following numerical examples. Given a domain  $\Omega \subset \mathbb{R}^3$  with boundary  $\Gamma = \partial\Omega$ , assume that  $\Gamma_D$  and  $\Gamma_N$  denote the Dirichlet part and Neumann part on the boundary. The strong form of governing equations in elasticity boundary value problem can be expressed as:

$$\begin{aligned}\nabla \boldsymbol{\sigma} + \mathbf{b} &= \mathbf{0} \\ \mathbf{u} &= \bar{\mathbf{g}} \\ \boldsymbol{\sigma} \cdot \mathbf{n} &= \bar{\mathbf{h}}\end{aligned}\quad (11)$$

where  $\bar{\mathbf{g}}$  and  $\bar{\mathbf{h}}$  denote the prescribed boundary displacement and traction,  $\mathbf{n}$  is the outer normal of the Neumann boundary and  $\mathbf{u}$  represents the displacement field. Under the assumption of elastic conditions and small displacement, the strain tensor  $\boldsymbol{\varepsilon}$  is defined by the symmetric part of the displacement gradient as:

$$\boldsymbol{\varepsilon} = 0.5(\nabla \mathbf{u} + \nabla^T \mathbf{u}) \quad (12)$$

The stress tensor  $\boldsymbol{\sigma}$  can be derived through the Hooke's law by:

$$\boldsymbol{\sigma} = \mathbf{D} : \boldsymbol{\varepsilon} \quad (13)$$

where  $\mathbf{D}$  is the elastic tangent matrix. Substituting Eqs. (12)-(13) into Eq. (11), the variation of governing equations in Eq. (11) can be rewritten in a weak form as follow:

$$\int_{\Omega} \delta \boldsymbol{\varepsilon} : \boldsymbol{\sigma} d\Omega = \int_{\Omega} \delta \mathbf{u} \cdot \mathbf{b} d\Omega + \int_{\Gamma_N} \delta \mathbf{u} \cdot \bar{\mathbf{h}} d\Gamma \quad (14)$$

In this work, Bernstein polynomials in representing geometrical models are regarded as the shape functions for isogeometric analysis. Hence, for each element the discretization of the geometry  $\mathbf{x}$  and displacement  $\mathbf{u}$  can be expressed by:

$$\mathbf{x}(u, v) = \sum_{i=1}^{ncp} B_i(u, v) \mathbf{P}_i \quad (15)$$

$$\mathbf{u}(u, v) = \sum_{i=1}^{ncp} B_i(u, v) \mathbf{d}_i \quad (16)$$

where  $(u, v)$  are the parameter coordinates of a point mapping from parent space to the parameter space. Parent space is developed from a generalized isoparametric element such as a square or a triangle.  $B_i(u, v)$  denote the Bernstein polynomials.  $\mathbf{P}_i$  and  $\mathbf{d}_i$  denote the control points of the geometry and the displacement, respectively.  $ncp$  is the number of the control points in an element which corresponds to a Bézier patch. For triangular Bézier element (patch), the parent element is a right triangle with three vertices  $(0, 0)$ ,  $(0, 1)$ ,  $(1, 0)$ . For quadrilateral Bézier element (patch), the parent element is a standard isoparametric element with domain  $[-1, 1] \otimes [-1, 1]$ . The standard and collapsed Gaussian quadrature rules [17] are implemented for numerical integration of quadrilateral and triangular Bézier patches.

## 6 NUMERICAL EXAMPLES

Two-dimensional elasticity problem, free vibration of Reissner-Mindlin plate and static bending of Reissner-Mindlin shell are investigated to verify the accuracy, convergence and validity of the presented method in this section. In two-dimensional models, the conversion is geometrically exact if we ignore the approximation error of trimming curves, which always exists in the CAD model. All the geometries are built in *Rhino* platform and exported as *.igs* files for mixed Bézier discretizations.

### 6.1 Infinite Plate with a Circular Hole

In the first example, a benchmark problem for stress distribution in an infinite plate with a circular hole is considered as illustrated in Fig. 12. The infinite plate is subjected to a uniform tension of magnitude  $T$  in the  $x$ -direction and a finite quarter plate is constructed for simulation due to the symmetry property. The exact solution of the stress tensor in a polar coordinate system  $(r, \theta)$  is given by [31]:

$$\begin{aligned}\sigma_{rr}(r, \theta) &= \frac{T}{2} \left[ 1 - \frac{a^2}{r^2} + \left( 1 + \frac{3a^4}{r^4} - \frac{4a^2}{r^2} \right) \cos 2\theta \right] \\ \sigma_{\theta\theta}(r, \theta) &= \frac{T}{2} \left[ 1 + \frac{a^2}{r^2} - \left( 1 + \frac{3a^4}{r^4} \right) \cos 2\theta \right] \\ \sigma_{r\theta}(r, \theta) &= -\frac{T}{2} \left( 1 - \frac{3a^4}{r^4} + \frac{2a^2}{r^2} \right) \sin 2\theta\end{aligned}\quad (17)$$

where  $a$  denotes the radius of the circular hole. As illustrated in Fig. 12(b), displacement boundary condition is symmetrically imposed on the left and bottom edges and traction boundary condition derived from exact stress tensor is enforced on the right and top edges.

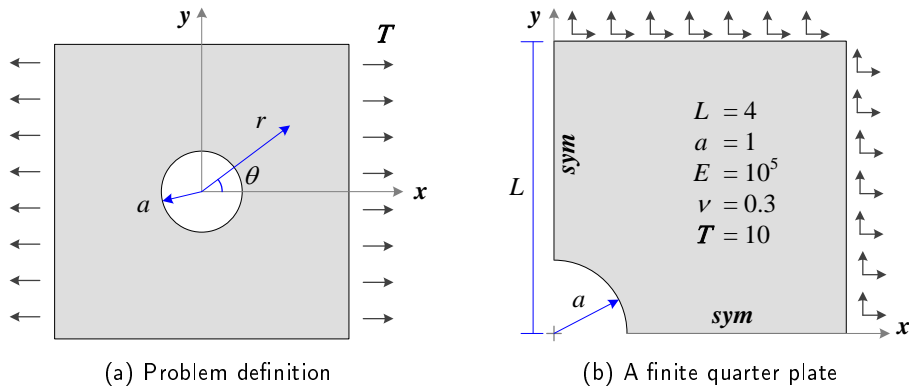


**Figure 12:** Infinite plate with a circular hole. (a) Problem definition and (b) a symmetric finite quarter plate for the problem.

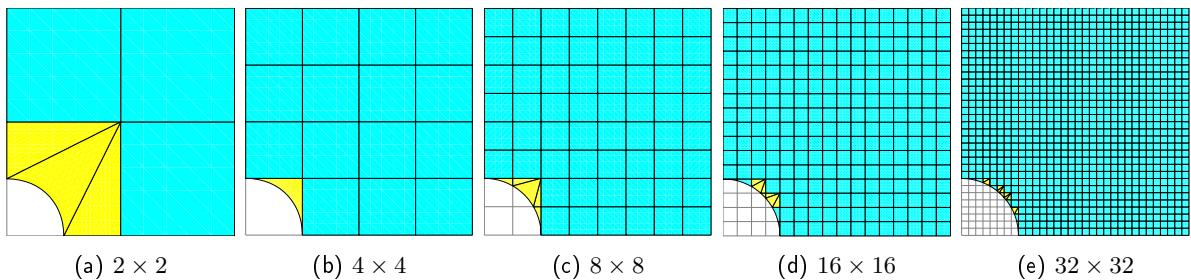


**Figure 13:** Mixed Bézier discretization from Trimmed NURBS with different mesh size. Yellow element denotes triangular Bézier patch and cyan element denotes tensor-product Bézier patch.

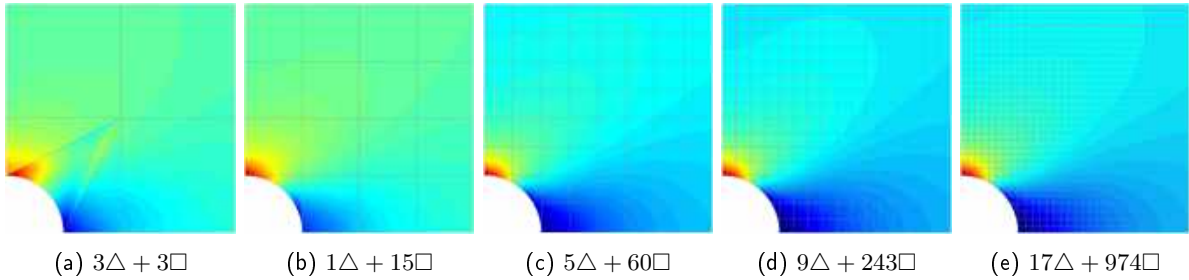


**Figure 14:** Stress  $\sigma_{xx}$  contour under different mixed Bézier discretizations given in Fig. 13.  $\triangle$  and  $\square$  denote the triangular Bézier patch and quadrilateral Bézier patch, e.g.,  $3\triangle+3\square$  means the mixed Bézier mesh consists of 3 triangular Bézier patches and 3 quadrilateral Bézier patches.

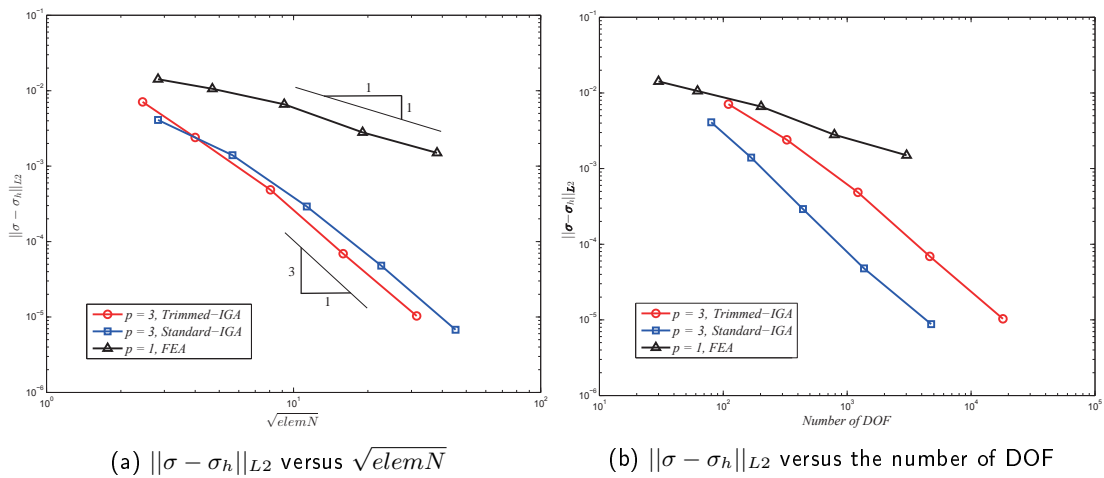


**Figure 15:** Comparison of convergence behaviors in the stress  $L_2$ -norm versus (a) the square root of number of elements  $\sqrt{elemN}$  and (b) the number of degrees of freedom. Lowercase  $p$  in legends denote the degree of elements (patches).

This problem is studied by using linear finite element method, standard cubic NURBS-based IGA and trimmed NURBS-based IGA. For finite element method, plate is automatically meshed into composition of triangles and quadrangles in ABAQUS. For standard NURBS-based IGA, plate is represented with only one untrimmed NURBS patch and uniformly refined with  $h$ -refinement strategy. Note that the standard NURBS-based IGA could be implemented by using an open-source toolbox NLIGA [8]. For trimmed NURBS based IGA, NURBS patch is constructed over the domain  $\Omega_{initial} = \{(x, y) | 0 \leq x \leq L, 0 \leq y \leq L\}$  and uniformly discretized into  $2 \times 2$ ,  $4 \times 4$ ,  $8 \times 8$ ,  $16 \times 16$ ,  $32 \times 32$  elements. To represent the plate model, a quarter of circle over the domain  $\Omega_{invalid} = \{(x, y) | x \geq 0, y \geq 0, x^2 + y^2 \leq a^2\}$  is trimmed off. Lastly the resulted trimmed-NURBS patch  $\Omega_{result}$  ( $\Omega_{result} = \Omega_{initial} - \Omega_{invalid}$ ) is converted into mixed Bézier patches (composition of triangular Bézier patches and quadrilateral Bézier patches), as presented in Fig. 13, where yellow elements denote the triangular Bézier patches and cyan elements denote the quadrilateral Bézier patches. Figure 14 shows the stress distribution under different mixed Bézier discretization given in Fig. 13. It can be found that stress is discontinuous along the interfaces in a very coarse mixed-Bézier model, e.g., in Figs. 14(a) and 14(b), and this discontinuity can be gradually alleviated with growth of Bézier patch number.

Convergence behaviors in the stress  $L_2$ -norm versus  $\sqrt{elemN}$  (the square root of number of elements) and the number of DOF (degree of freedom) with different mesh density are shown in Fig. 15. It can be noticed that both standard untrimmed bi-cubic NURBS and trimmed bi-cubic NURBS plates can converge with a same rate  $O(h^3)$  as depicted in Fig. 15(a), since the convergence rate is determined by the degree. The numerical results of trimmed NURBS are slightly more accurate than that of untrimmed NURBS when the sum of elements is more than a certain number, e.g.,  $\sqrt{elemN} > 4$  in Fig. 15(a). The reason is that, in the same mesh density, the converted  $C^0$ -continuity mixed Bézier patches from trimmed NURBS will produce more control variables (or DOFs) than  $C^2$ -continuity untrimmed NURBS. As plotted in Fig. 15(b), the results obtained from untrimmed NURBS are more accurate than that of converted mixed Bézier patches in the same number of DOFs as given in Fig. 15(b), even though they converge with almost the same rate. It can be concluded that the higher smoothness of the untrimmed NURBS leads to a better/lower constant in the error estimator, leading to the offset in favor of the smooth discretization.

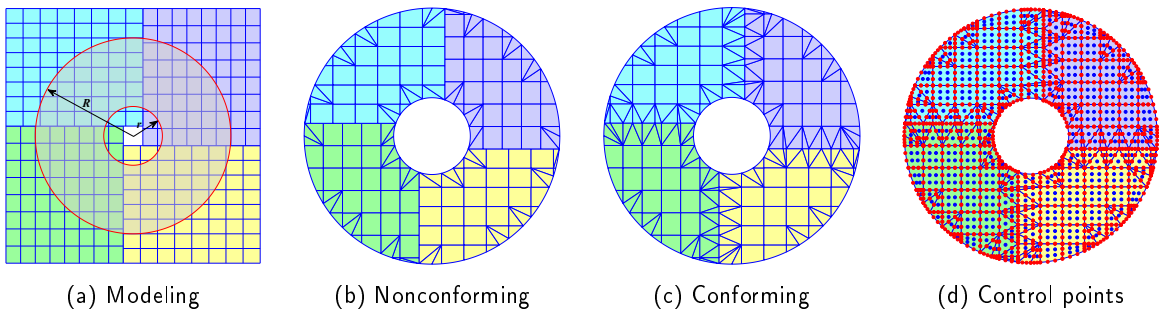


**Figure 16:** Annular plate modeling and discretization,  $r/R = 0.3$ . (a) Annular is trimmed from square plate with a square hole constructed by four nonconforming NURBS patches. (b) and (c) are the nonconforming and conforming discretization of the annular plate. (d) Control points of the conforming mixed Bézier model are displayed.

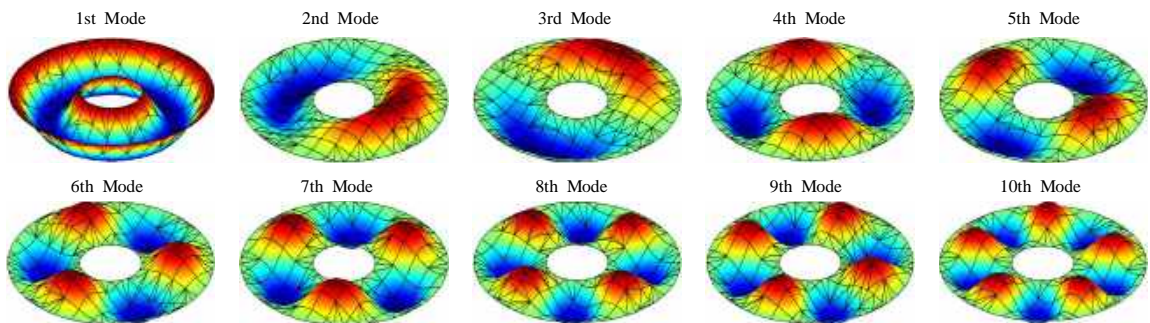


**Figure 17:** The first ten Mode shapes of trimmed annular plate with both clamped inner and outer edges,  $h/R = 0.1, r/R = 0.3$ .

## 6.2 Free Vibration of an Annular Plate Built with Four Trimmed Patches

In this example, we want to discuss the application of mixed Bézier discretization on trimmed multi-patch NURBS objects. The annular plate is only built with a singular trimmed patch in previous example, while



**Table 1:** Comparison of frequency parameters,  $\varpi = \omega R^2 \sqrt{\rho h / D_0}$ , for thick annular plates with both clamped inner and outer edges,  $h/R = 0.1$  and  $r/R = 0.3, 0.5$ .

$r/R$	Method	Mode types					
		(0,1)	(0,2)	(1,1)	(1,2)	(2,1)	(2,2)
0.3	Irie [14]	39.40	95.59	40.37	96.99	43.98	101.43
	Standard-IGA	39.4581	95.8365	40.4310	97.2368	44.0459	101.6798
	Trimmed-IGA	39.4614	95.8597	40.4357	97.2640	44.0529	101.7169
0.5	Irie [14]	70.28	159.78	70.90	160.60	72.96	163.08
	Standard-IGA	70.4426	160.3419	71.0711	161.1597	73.1354	163.6483
	Trimmed-IGA	70.4537	160.5698	71.0838	161.3910	73.1513	163.8062

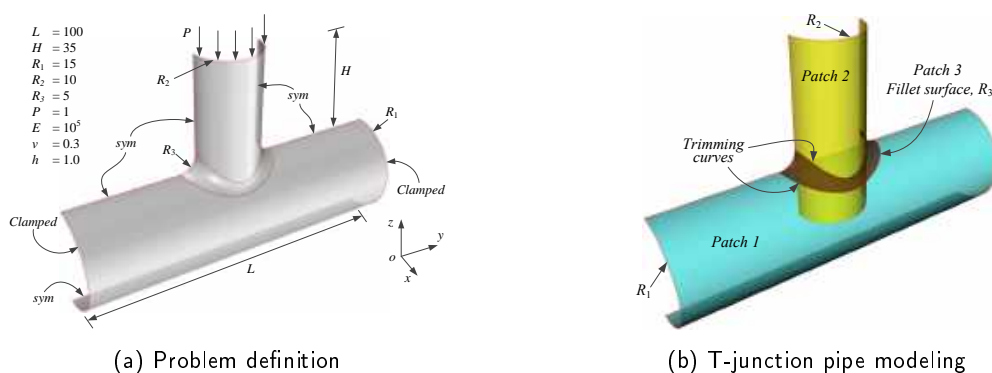


**Figure 18:** Problem definition and modeling of the T-junction pipe.

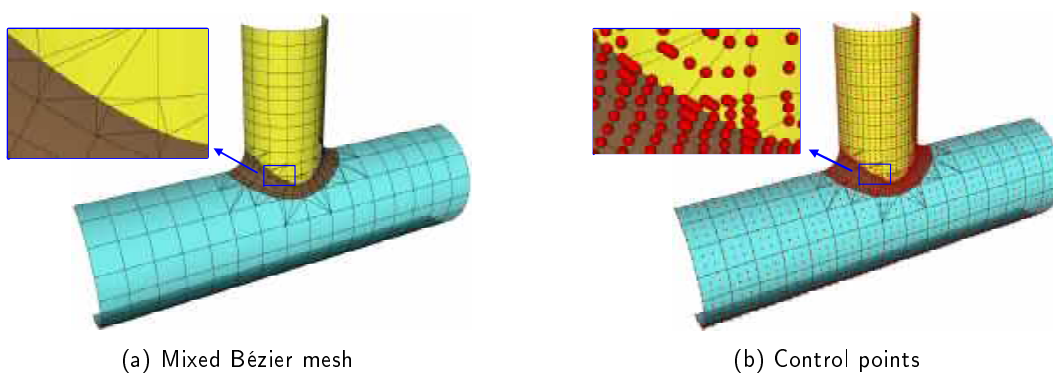


**Figure 19:** Discretizations of multi-trimmed T-junction pipe model.

here it is built with four non-conforming trimmed patches. Just like the previous example, two radius-ratios  $r/R = 0.3, 0.5$  and thickness-span ratio  $h/R = 0.1$  are considered. The original square plate with a small square hole is firstly modeled by four non-conforming NURBS patches and then is trimmed by two circles with radius  $r$  and  $R$  as shown in Fig. 16(a). The nonconforming and conforming mixed-Bézier discretization are given in Figs. 16(b) and 16(c) where conforming discretization consists of 189 triangular Bézier patches and 60 rectangular Bézier patches for radius-ratio  $r/R = 0.3$ . Meanwhile, it consists of 173 triangular Bézier patches and 48 rectangular Bézier patches for radius-ratio  $r/R = 0.5$ . Figure 16(d) shows control points for the conforming mixed-Bézier discretization.

Inner and outer edges are both clamped as boundary condition for free vibration analysis. As listed in table 1, the dimensionless frequency parameter  $\varpi = \omega R^2 \sqrt{\rho h / D_0}$  is calculated for the annular plate with radius-ratios  $r/R = 0.3, 0.5$ . The existing results in [14] and the results obtained from an untrimmed annular plate are also listed for comparison. It can be found that these results agree well with each other. In addition, the first ten mode shapes of the annular plate with  $h/R = 0.1, r/R = 0.3$  are plotted in Fig. 17.

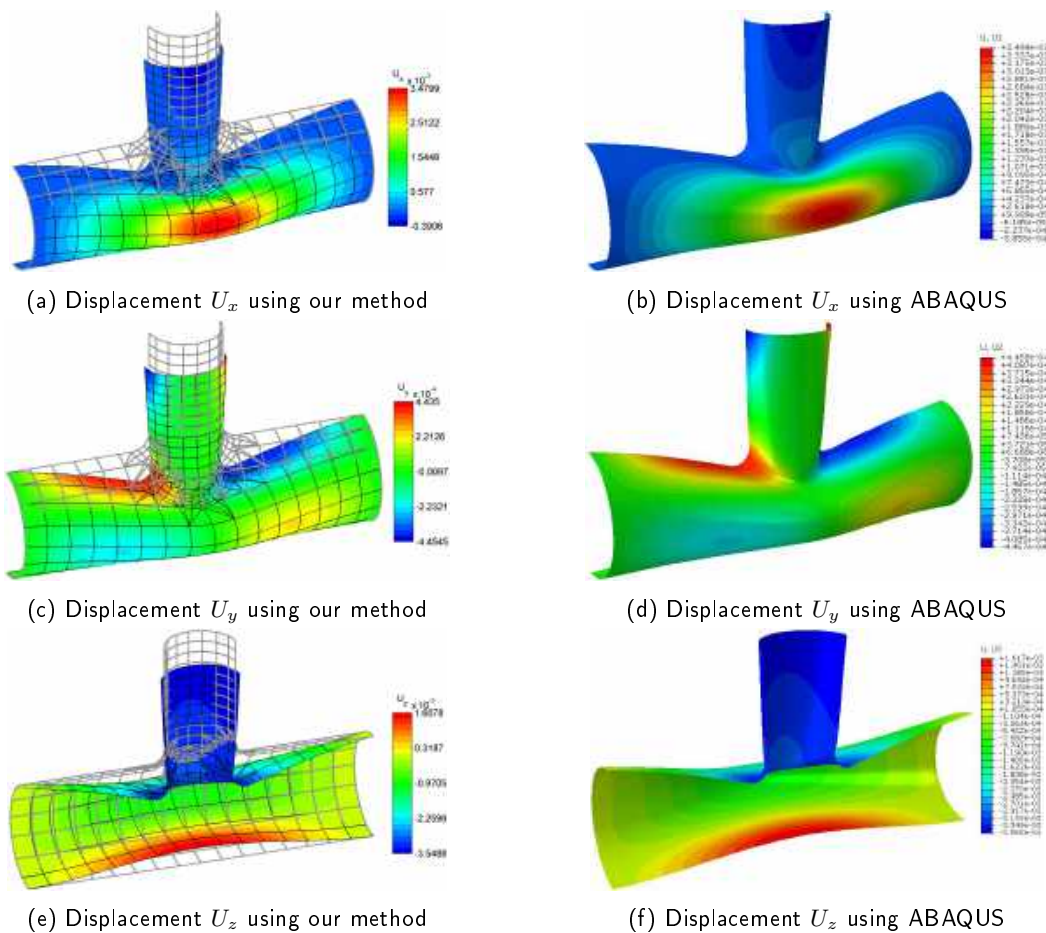


**Figure 20:** Displacement contours of T-junction-pipe shell under a uniform edge load  $P$  obtained by using our method and ABAQUS.

### 6.3 T-junction Pipe

In this example, we consider a multi-trimmed T-junction pipe shell problem based on the Reissner-Mindlin shell theory. The T-junction pipe is built with two orthogonally intersected pipe and the interface of the pipes is filleted. Due to the symmetry property, a half of the T-junction pipe is modeled with three NURBS patches as depicted in Fig. 18(a). The edges of the horizontal pipe are clamped and the top edge of the vertical pipe is subjected to an edge load  $P$ . As illustrated in Fig. 18(b), a fillet surface  $R_3$  is generated from the interface of the intersected semi-cylindrical patch 1 with radius  $R_1$  and semi-cylindrical patch 2 with radius  $R_2$ . It should be noticed that the fillet surface is tangent to both patch 1 and patch 2. Two boundary curves of the fillet surface is also regarded as the trimming boundaries of patch 1 and patch 2. Therefore, both patch 1 and patch 2 are trimmed surfaces.

Multi-trimmed T-junction pipe model is discretized into 242 bi-cubic quadrilateral Bézier patches and 116 cubic triangular Bézier patches as shown in Fig. 19. The number of control points is 2821 in total. Two blown-up views are given to show the local details of the discretization. Reissner-Mindlin shell theory is employed to study the deformation of the pipe model. Material properties are  $E = 1 \times 10^5$ ,  $\nu = 0.3$  and thickness  $h = 1.0$ . Figure 20 presents the comparison of displacement in three directions between present results and that of ABAQUS where the T-junction pipe is discretized into 22246 quadratic shell elements and 67309 nodes to calculate the displacement results. To better visualize the displacement contour, a deformation scale factor  $f = 2.8476 \times 10^3$  is applied on the deformed model. Gray grids on the contours denote the un-deformed Bézier meshes. The present results are found in good coincidence with that of ABAQUS from the comparison. In addition, the displacement of edges is projected to the  $y$ - $z$  plane with  $x = 0.0$ , as plotted in Fig. 21, to observe the deformation result differences between the present trimmed-IGA method and finite element method in ABAQUS.

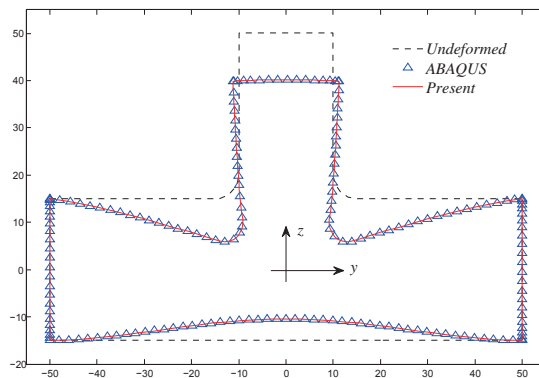


**Figure 21:** Projection of displacement on the boundaries to the  $y$ - $z$  plane with  $x = 0.0$ . The results of present method are compared with that of ABAQUS and the undeformed boundaries. The deformation scale factor is  $2.8476 \times 10^3$ .

## 7 CONCLUSIONS

Various problems including enforcement of Dirichlet boundary conditions, conforming of trimming interfaces and quadrature of trimmed elements will be encountered when implementing isogeometric analysis on trimmed models which are ubiquitous in the field of computer-aided geometric design. To bypass these tricky problems, in this paper, a novel approach is proposed to convert the trimmed surfaces into mixed Bézier patches for isogeometric analysis. The converted models are watertight and can keep the original model geometrically

exact except the parts along the narrow area of trimming curves, where the approximated error depends on the flatness of the trimmed elements and can be reduced by refining the NURBS surface with knot insertion algorithm. The comparison of presented results and that of ABAQUS or existing literatures shows the validity of the proposed method. Though this method tends to result an increase of DOFs in the resulting simulations, it intrinsically inherits the CAD structure of the original model so it's tightly compatible with the existing CAD representations, and as a result, the Bézier patch model can avoid the heavy burden of mesh repair work which is typical of FEA procedure and often arising from the damage of CAD information. Note that only  $C^0$  continuity across boundaries of Bézier patches is preserved. Therefore, future works will focus on the improvement of the continuity between Bézier patches especially the patches that are away from the narrow trimming area.

## ACKNOWLEDGEMENTS

The work is supported by the Natural Science Foundation of China (Project Nos. 61572056 and 61972011).

## ORCID

Xiaoxiao Du, <http://orcid.org/0000-0002-2324-1005>

## REFERENCES

- [1] Beer, G.; Marussig, B.; Zechner, J.: A simple approach to the numerical simulation with trimmed CAD surfaces. *Computer Methods in Applied Mechanics and Engineering*, 285, 776–790, 2015. <http://doi.org/10.1016/j.cma.2014.12.010>.
- [2] Breitenberger, M.; Apostolatos, A.; Philipp, B.; Wüchner, R.; Bletzinger, K.U.: Analysis in computer aided design: Nonlinear isogeometric B-Rep analysis of shell structures. *Computer Methods in Applied Mechanics and Engineering*, 284, 401–457, 2015. <http://doi.org/10.1016/j.cma.2014.09.033>.
- [3] Buffa, A.; Puppi, R.; Vázquez, R.: A minimal stabilization procedure for isogeometric methods on trimmed geometries. *arXiv preprint arXiv:1902.04937*, 2019.
- [4] Coox, L.; Greco, F.; Atak, O.; Vandepitte, D.; Desmet, W.: A robust patch coupling method for NURBS-based isogeometric analysis of non-conforming multipatch surfaces. *Computer Methods in Applied Mechanics and Engineering*, 316, 235–260, 2017. <http://doi.org/10.1016/j.cma.2016.06.022>.
- [5] Cottrell, J.A.; Hughes, T.J.; Bazilevs, Y.: *Isogeometric analysis: toward integration of CAD and FEA*. John Wiley & Sons, 2009. <http://doi.org/10.1002/9780470749081>.
- [6] Du, X.; Zhao, G.; Wang, W.: Nitsche method for isogeometric analysis of Reissner–Mindlin plate with non-conforming multi-patches. *Computer Aided Geometric Design*, 35, 121–136, 2015. <http://doi.org/10.1016/j.cagd.2015.03.005>.
- [7] Du, X.; Zhao, G.; Wang, W.; Fang, H.: Nitsche's method for non-conforming multipatch coupling in hyperelastic isogeometric analysis. *Computational Mechanics*, 65, 687–710, 2020. <http://doi.org/10.1007/s00466-019-01789-x>.
- [8] Du, X.; Zhao, G.; Wang, W.; Guo, M.; Zhang, R.; Yang, J.: Nliga: A matlab framework for nonlinear isogeometric analysis. *Computer Aided Geometric Design*, 80, 101869, 2020. <http://doi.org/10.1016/j.cagd.2020.101869>.
- [9] Engvall, L.; Evans, J.A.: Isogeometric unstructured tetrahedral and mixed-element Bernstein–Bézier discretizations. *Computer Methods in Applied Mechanics and Engineering*, 319, 83–123, 2017. <http://doi.org/10.1016/j.cma.2017.02.017>.

- [10] Farin, G.; Hansford, D.: Discrete Coons patches. *Computer Aided Geometric Design*, 16(7), 691–700, 1999. [http://doi.org/10.1016/S0167-8396\(99\)00031-X](http://doi.org/10.1016/S0167-8396(99)00031-X).
- [11] Farin, G.E.: *Curves and surfaces for CAGD: a practical guide*. Morgan Kaufmann, 2002. <http://doi.org/10.1016/B978-1-55860-737-8.X5000-5>.
- [12] Farouki, R.T.: The Bernstein polynomial basis: A centennial retrospective. *Computer Aided Geometric Design*, 29(6), 379–419, 2012. <http://doi.org/10.1016/j.cagd.2012.03.001>.
- [13] Hughes, T.J.; Cottrell, J.A.; Bazilevs, Y.: Isogeometric analysis: CAD, finite elements, NURBS, exact geometry and mesh refinement. *Computer methods in applied mechanics and engineering*, 194(39), 4135–4195, 2005. <http://doi.org/10.1016/j.cma.2004.10.008>.
- [14] Irie, T.; Yamada, G.; Takagi, K.: Natural frequencies of thick annular plates. *Journal of Applied Mechanics*, 49(3), 633–638, 1982. <http://doi.org/10.1115/1.3162539>.
- [15] Kim, H.J.; Seo, Y.D.; Youn, S.K.: Isogeometric analysis for trimmed CAD surfaces. *Computer Methods in Applied Mechanics and Engineering*, 198(37), 2982–2995, 2009. <http://doi.org/10.1016/j.cma.2009.05.004>.
- [16] Kim, H.J.; Seo, Y.D.; Youn, S.K.: Isogeometric analysis with trimming technique for problems of arbitrary complex topology. *Computer Methods in Applied Mechanics and Engineering*, 199(45), 2796–2812, 2010. <http://doi.org/10.1016/j.cma.2010.04.015>.
- [17] Lyness, J.N.; Cools, R.: A survey of numerical cubature over triangles. In *Proceedings of Symposia in Applied Mathematics*, vol. 48, 127–150, 1994. <http://doi.org/10.1090/psapm/048/1314845>.
- [18] Marussig, B.; Hughes, T.J.: A review of trimming in isogeometric analysis: challenges, data exchange and simulation aspects. *Archives of computational methods in engineering*, 25(4), 1059–1127, 2018. <http://doi.org/10.1007/s11831-017-9220-9>.
- [19] Marussig, B.; Zechner, J.; Beer, G.; Fries, T.P.: Stable isogeometric analysis of trimmed geometries. *Computer Methods in Applied Mechanics and Engineering*, 316, 497–521, 2017. <http://doi.org/10.1016/j.cma.2016.07.040>.
- [20] Nagy, A.P.; Benson, D.J.: On the numerical integration of trimmed isogeometric elements. *Computer Methods in Applied Mechanics and Engineering*, 284, 165–185, 2015. <http://doi.org/10.1016/j.cma.2014.08.002>.
- [21] Philipp, B.; Breitenberger, M.; D’Auria, I.; Wüchner, R.; Bletzinger, K.U.: Integrated design and analysis of structural membranes using the isogeometric B-Rep analysis. *Computer Methods in Applied Mechanics and Engineering*, 303, 312–340, 2016. <http://doi.org/10.1016/j.cma.2016.02.003>.
- [22] Piegl, L.; Tiller, W.: *The NURBS Book*, 2nd ed. Springer Berlin Heidelberg, 1997.
- [23] Renner, G.; Weiss, V.: Exact and approximate computation of B-spline curves on surfaces. *Computer-Aided Design*, 36(4), 351–362, 2004. [http://doi.org/10.1016/S0010-4485\(03\)00100-3](http://doi.org/10.1016/S0010-4485(03)00100-3).
- [24] Ruess, M.; Schillinger, D.; Özcan, A.I.; Rank, E.: Weak coupling for isogeometric analysis of non-matching and trimmed multi-patch geometries. *Computer Methods in Applied Mechanics and Engineering*, 269, 46–71, 2014. <http://doi.org/10.1016/j.cma.2013.10.009>.
- [25] Schillinger, D.; Ruess, M.: The finite cell method: a review in the context of higher-order structural analysis of CAD and image-based geometric models. *Archives of Computational Methods in Engineering*, 22(3), 391–455, 2015. <http://doi.org/10.1007/s11831-014-9115-y>.
- [26] Schmidt, R.; Wüchner, R.; Bletzinger, K.U.: Isogeometric analysis of trimmed NURBS geometries. *Computer Methods in Applied Mechanics and Engineering*, 241, 93–111, 2012. <http://doi.org/10.1016/j.cma.2012.05.021>.
- [27] Sederberg, T.W.; Anderson, D.C.; Goldman, R.N.: Implicit representation of parametric curves and

- surfaces. *Computer Vision, Graphics, and Image Processing*, 28(1), 72–84, 1984. [http://doi.org/10.1016/0734-189X\(84\)90140-3](http://doi.org/10.1016/0734-189X(84)90140-3).
- [28] Sevilla, R.; Fernández-Méndez, S.; Huerta, A.: NURBS-enhanced finite element method (NEFEM). *International Journal for Numerical Methods in Engineering*, 76(1), 56–83, 2008. <http://doi.org/10.1002/nme.2311>.
- [29] Thomas, D.; Engvall, L.; Schmidt, S.; Tew, K.; Scott, M.: U-splines: Splines over unstructured meshes. <https://coreform.com/usplines>, 2018.
- [30] Thomas, D.C.; Scott, M.A.; Evans, J.A.; Tew, K.; Evans, E.J.: Bézier projection: a unified approach for local projection and quadrature-free refinement and coarsening of NURBS and T-splines with particular application to isogeometric design and analysis. *Computer Methods in Applied Mechanics and Engineering*, 284, 55–105, 2015. <http://doi.org/10.1016/j.cma.2014.07.014>.
- [31] Timoshenko, S.; Goodier, J.N.: *Theory of elasticity*. McGraw-Hill Book Company Inc, 1951.
- [32] Vlachos, A.; Peters, J.; Boyd, C.; Mitchell, J.L.: Curved PN triangles. In *Proceedings of the 2001 symposium on Interactive 3D graphics*, 159–166. ACM, 2001. <http://doi.org/10.1145/364338.364387>.
- [33] Wang, Y.W.; Huang, Z.D.; Zheng, Y.; Zhang, S.G.: Isogeometric analysis for compound B-spline surfaces. *Computer Methods in Applied Mechanics and Engineering*, 261, 1–15, 2013. <http://doi.org/10.1016/j.cma.2013.04.001>.
- [34] Xia, S.; Qian, X.: Isogeometric analysis with Bézier tetrahedra. *Computer Methods in Applied Mechanics and Engineering*, 316, 782–816, 2017. <http://doi.org/10.1016/j.cma.2016.09.045>.
- [35] Xia, S.; Wang, X.; Qian, X.: Continuity and convergence in rational triangular Bézier spline based isogeometric analysis. *Computer Methods in Applied Mechanics and Engineering*, 297, 292–324, 2015. <http://doi.org/10.1016/j.cma.2015.09.001>.
- [36] Xu, G.; Mourrain, B.; Duvigneau, R.; Galligo, A.: Parameterization of computational domain in isogeometric analysis: methods and comparison. *Computer Methods in Applied Mechanics and Engineering*, 200(23), 2021–2031, 2011. <http://doi.org/10.1016/j.cma.2011.03.005>.
- [37] Xu, G.; Mourrain, B.; Duvigneau, R.; Galligo, A.: Optimal analysis-aware parameterization of computational domain in 3D isogeometric analysis. *Computer-Aided Design*, 45(4), 812–821, 2013. <http://doi.org/10.1016/j.cad.2011.05.007>.
- [38] Xu, J.; Sun, N.; Shu, L.; Rabczuk, T.; Xu, G.: An improved isogeometric analysis method for trimmed geometries. *arXiv preprint arXiv:1707.00323*, 2017.
- [39] Zhao, G.; Du, X.; Wang, W.; Liu, B.; Fang, H.: Application of isogeometric method to free vibration of Reissner–Mindlin plates with non-conforming multi-patch. *Computer-Aided Design*, 82, 127–139, 2017. <http://doi.org/10.1016/j.cad.2016.04.006>.
- [40] Zhu, X.; Hu, P.; Ma, Z.D.: B++ splines with applications to isogeometric analysis. *Computer Methods in Applied Mechanics and Engineering*, 311, 503–536, 2016. <http://doi.org/10.1016/j.cma.2016.08.029>.